Sensors and Actuators A 323 (2021) 112649

Contents lists available at ScienceDirect

Sensors and Actuators A: Physical

journal homepage: www.elsevier.com/locate/sna

Piezoelectric titanium based microfluidic pump and valves for implantable medical applications

Agnes Beate Bußmann [a,b,*,1], Claudia Patricia Durasiewicz [a,c,*,1], Sebastian Heinrich Alexander Kibler [a], Christian Klaus Wald [a]

[a] Fraunhofer EMFT Research Institution for Microsystems and Solid State Technologies, Hansastrasse 27d, 80686, Munich, Germany
[b] KIT, MAB - Biomolecular Separation Engineering, Fritz-Haber-Weg 2, 76131, Karlsruhe, Germany
[c] TUM, TEP - Chair of Physics of Electrotechnology, Theresienstrasse 90, 80333, Munich, Germany

ARTICLE INFO

Article history:
Received 9 November 2020
Received in revised form 15 January 2021
Accepted 19 February 2021
Available online 26 February 2021

Keywords:
Micropump
Microvalve
Titanium
Piezoelectric bending actuator
Microfluidic system
Microfluidic implant

ABSTRACT

Medical devices often require precise movement of fluids. Automated implants with no need for manual handling improve patient care significantly. However, existing microfluidic devices do not fulfil the necessary specifications of size, safety, hermetic sealing, and artefact free medical imaging, as well as energy efficiency combined with adapted fluidic properties. In this work we designed, manufactured, and experimentally evaluated three piezoelectric microfluidic devices for implant automation: a diaphragm pump, a normally closed valve, and a normally open valve. All devices are made of titanium, minimizing the risk of artefacts in medical imaging. They have similar form factors and use the same actuation method. For the later, a specific mounting process of the piezo actuator enables outstanding fluidic performance during experimental evaluations. The titanium micropumps show a maximal flow of (14 ± 2.2) ml/min and pressure build-up of 75 kPa. The normally closed valve's leakage rates are extremely low with less than 1 µL/min. Detailed investigations further include the actuator stroke, a lifetime study for normally open valves, and a numerical and experimental evaluation of the normally closed valve's spring foil. The introduced titanium technology platform is ideally suited for system integration accounted for by the use of the same actuation principle and the similar form factor and a simple design. The development of small, smart, and energy efficient implants for improved treatment is possible based on the introduced platform.

1. Introduction

The transport of liquids is an ubiquitous task in implantable medical applications. Examples are, among others, microfluidic systems to move body fluids, dose medication precisely, or hydraulic implants [1–3]. Prosthetic hands [4], extra-aortic balloon (EAB) pumps [5], as well as artificial sphincters base on hydraulic actuation. These implants can be realized using flexible, fluid-filled actuators, such as artificial fingers [4], or a cuff placed around a vessel or muscular tube, to facilitate a biological function. The actuators are operated using intra- or extracorporeal pumps and/or valves. Cuffs in EAB devices are dynamically pressurized by extracorporeal pumps to levels of 250–300 mmHg (333–400 mbar), providing cardiac support by increased blood flow for patients suffering from heart failure [5]. However, current systems are too large for implantation. Sphincter implants [6,7] restore opening and closing functionalities in the rectal or urinary path. Current systems on the market are manual devices which the patient operates by hand. Furthermore, the physician sets the pressure to a fixed level that is not adapted to the patient's activity, which can cause tissue damage. Even if specifications vary largely with the use case, a small, light, automated, and user-friendly device is desired for future developments of implants. Ever since the first studies on piezoelectric diaphragm pumps [8], many different kinds of micropumps have been developed to enable reliable, safe, and economic medical products [9,10].

Micropumps in research achieve water flow rates of up to 9.1 mL/min or water pressures of up to 40 kPa, though fail to exhibit high flow and pressure simultaneously [11]. Additionally, the

Abbreviations: EAB, extra-aortic balloon; FEM, finite-element-modelling; FKM, fluorocarbon; MRI, magnetic resonance imaging; NC, normally closed; NO, normally open.

* Corresponding authors at: Fraunhofer EMFT Research Institution for Microsystems and Solid State Technologies, Hansastrasse 27d, 80686, Munich, Germany.
E-mail addresses: Agnes.Bussmann@emft.fraunhofer.de (A.B. Bußmann), Claudia.Patricia.Durasiewicz@emft.fraunhofer.de (C.P. Durasiewicz).
[1] A. Bußmann and C. Durasiewicz contributed equally.

https://doi.org/10.1016/j.sna.2021.112649

occurrence of bubbles due to degassing or cavitation [12] impacts the fluidic performance. For safety reasons, medical applications require bubble tolerance, even under backpressure. We therefore seek to develop a high performance micropump with bubble tolerance capabilities. This is ensured by an adapted design including a large compression ratio (ratio of displaced volume to dead volume in the pump chamber [13]). A high ratio can be achieved by a specific mounting procedure for the piezo ceramic: a voltage, applied during glue hardening, causes the actuator diaphragm to permanently bulge out, creating the pump chamber [14]. The achieved compression ratio leads to a high pressure build-up with air and enables bubble tolerance.

Microvalves are an important additional component for implantable applications, for instance as a safety measure. Based on different actuation methods, e.g., piezoelectric, shape memory alloy, electrostatic, or magnetic, various types of microvalves have been developed [15,16]. The two basic groups of valves are normally closed (NC) and normally open (NO) valves. NC valves block the fluidic path, only opening when actuated. By contrast, NO valves allow flow while not actuated and are actively closed. Both types offer adapted properties for different applications. Examples of piezoelectric valves are presented in research [17–19]. Water leakage rates as low as 0.013 μL/min [20] and water free flow of up to 8.75 mL/min [21] are achieved. In contrast to existing microvalves, we want to combine low leakage of a soft sealing on a solid valve seat with a large free flow operating range. Valves are designed to benefit from the high force and fast response time abilities of piezoelectric actuation, which allows their usage in challenging flow conditions such as high differential pressure.

Fluidic conditions are not the only demanding aspect in microfluidic systems. The electrical system needs to be hermetically sealed from the fluid path to prevent damage. Use within the human body requires additional sealing, and every material in contact with tissue has to be biocompatible. Metal pumps, such as stainless steel pumps [22,23], offer welding as possible hermetic sealing. However, stainless steel has a large disadvantage when it comes to long-term medical implants: this material causes artifacts in magnetic resonance imaging (MRI) scanning, as evaluations on different implants have shown [24–26]. A suitable material to solve this issue is titanium, which offers numerous advantages for use in medical applications [27] in addition to its MRI compatibility: When exposed to air, its surface forms biocompatible and antibacterial titanium dioxide [28,29]. Titanium components can be hermetically sealed from the human body, e.g., by welding titanium covers to them [30]. Since no different materials are bonded together, the risk of galvanic corrosion is minimized [31]. So far there are examples of micropumps and valves partly manufactured of titanium [32–35].

In our work, we develop a titanium platform of microfluidic devices for medical implants. It includes new designs of a NO valve and a NC valve, making use of the beneficial properties of titanium. In addition, we adapt the proven design of known steel micropumps [22] to titanium. The small and light devices are designed to allow easy integration into efficient products. These automated solutions aim to increase patients' comfort.

2. Micropump and valve design

Hydraulic actuators usually rely on a combination of pumps and valves. For microfluidic implants, many combinations are imaginable and design strongly depends on the exact use case. Fig. 1 depicts a generalized fluidic setup for hydraulic actuation. The pump actively transports fluid from P1 to P2 and builds up a pressure, while an active valve maintains or releases the pressure as needed. P1 and P2 are volumes that can either be the hydraulically actuated part or a fluid reservoir. In case of a malfunction such as the loss of power, the implant has to remain in a safe state, where any critical pressure is released to prevent risk of injury. Therefore, depending on the exact design, e.g., a pressurized or non-pressurized reservoir, the use of a NO or NC valve is required. A NO valve ensures pressure release in non-actuated state, for a hydraulically actuated volume at P2 where a permanently applied pressure can cause injury. Whereas if a constant pressure is unproblematic regarding safety aspects, a NC valve can be used to enable a more energy efficient use.

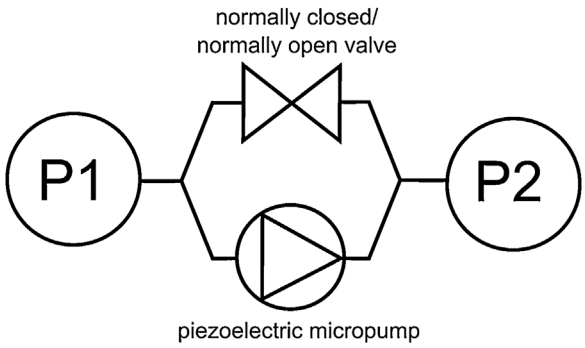

Fig. 1. Fluidic setup of a hydraulic actuation unit. The pump transports fluid between a reservoir and the actuated part, which are depicted as P1 and P2 here. The valve can maintain and release the built up pressure as required. Different working principles achieved with alternative circuit arrangements are possible. The decision for a normally closed or a normally open valve depends, among others, on safety aspects, since a pressure release of the actuated part in the case of power loss is often necessary.

In general, piezoelectric actuation allows for energy efficient driving (v.i., "Experimental Results and Discussion") [9]. Even a NO valve, operated to be closed most of the time, does not require excessive energy, since the piezoelectric ceramic acts as a capacitance and leakage currents are low. Hence, the applied voltage remains stable over long periods. Therefore, this titanium technology platform enables the development of space and energy efficient products.

For easy combination, we design the three devices to use the same actuation principle, be manufactured in similar processes, and be geometrically alike. Titanium and FKM, the wetted materials of the microfluidic devices developed, were sourced in medical grade. Those materials exhibit beneficial traits and are already used in medical devices. However, a detailed biocompatibility testing is necessary and not yet part of this study, which focuses on the technical development. Since the hydraulic fluid system is a closed circuit setup, contact to the body does not occur during orderly function. A critical element is the piezoelectric actuator. The lead content as well as the electric contact makes hermetic sealing and electric isolation indispensable. The devices are designed to allow such sealing, e.g., by laser welding.

2.1. Titanium pump

The design of the titanium micro diaphragm pump (Fig. 2a) is similar to our steel pumps [22]. The pump includes a titanium body in combination with a glued on piezoelectric disc actuator (PIC 151, d = 16 mm; 200 μm) (Fig. 2c). The body consists of a base plate and three titanium foils: two valve foils and one actuator foil. All metal parts are laser welded to form the impermeable pump chamber. The current device has a diameter of 20 mm and a height of 1.5 mm.

Pumping bases on the indirect piezoelectric effect, causing a mechanical deformation when the piezoelectric ceramic is exposed to electrical actuation. Hence, applying an alternating high voltage signal results in an oscillating vertical diaphragm deflection

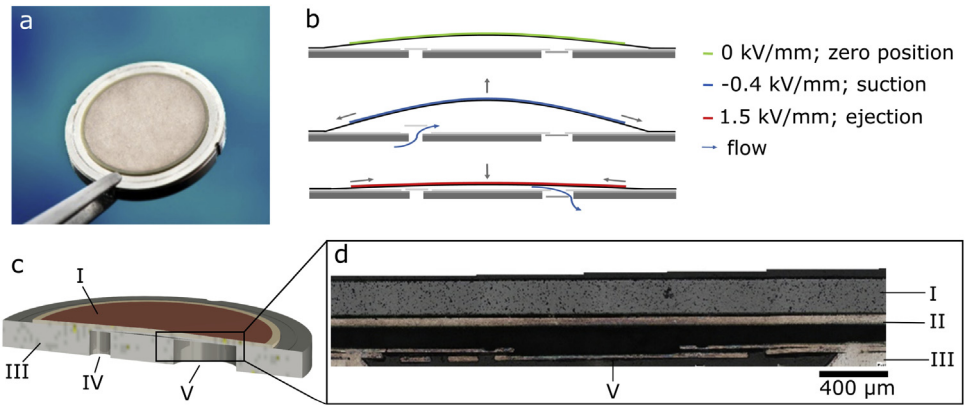

Fig. 2. **a** Picture of a piezoelectric titanium micropump. **b** working principle. Due to the indirect piezoelectric effect, an alternating high voltage causes an oscillating movement of diaphragm. In combination with two passive spring valves, this leads to an effective flow. **c** model of the pump showing the piezo actuator (I), the pump body (III), the inlet (IV) and outlet (V). **d** section of the outlet valve (V) welded to the pump body (III) with piezo ceramic (I) glued to the actuator diaphragm (II).

and creates a fluid movement through two passive spring valves (Fig. 2b).

The pretension technique [36] for piezo mounting promotes a high pumping performance. The ceramic is exposed to a defined electric field while curing the glue. Therefore, bonding takes place in a contracted state of the piezo. After curing, the voltage is removed and the expansion of the ceramic bulges out the pump chamber. This specific mounting establishes a large compression ratio (displaced volume / dead volume) and therefore leads to self-priming and bubble tolerant pumps up to at least 30 kPa.

2.2. Normally open valve

The design of the titanium NO valve is similar to the titanium pumps, though the passive check valves are omitted (Fig. 3a). The bending actuator is a 100 µm titanium foil with a glued on piezo ceramic (PIC 151, d =16 mm; 200 µm). It is laser welded to the valve body, which includes two drilled openings for valve inlet and outlet. An O-ring soft sealing (medical grade FKM, nominal thickness of 500 µm), integrated into the valve body before laser welding, enables low leakage rates. The current device has a diameter of 20 mm and a height of 2.6 mm.

During non-actuated mode, fluid can pass through the clearance between the soft sealing and actuator membrane of the NO valve (Fig. 3). Exposure of the piezo ceramic to an electrical field causes a deflection towards the valve chamber bottom. Eventually, the diaphragm compresses the O-ring and blocks fluid movement (Fig. 3b). The pretension technique for piezo mounting is the driving factor for the valves' fluidic performance in its open state. It adjusts the chamber height and therefore determines the valve's fluidic resistance. Blocking is ensured as long as the actuator's force is greater than the force introduced to the membrane by fluid pressure. The NO valves use the same bending actuator as the titanium pumps and therefore overcome a minimal pressure of 80 kPa.

2.3. Normally closed valve

While the overall setup of the normally closed valve is more complex (Fig. 4a and b), its bending actuator is the same as for the pumps and NO valves. The NC valve includes an O-ring (medical grade FKM, nominal thickness of 500 µm) that is integrated into the valve's body. The soft sealing is compressed by a plunger, suspended by a 50 µm thin spring foil that pulls it upwards. The current device has a diameter of 20 mm and a height of 3.6 mm.

For manufacturing, the plunger is inserted in the valve body from beneath, bringing it into contact with the soft sealing. The spring foil is welded to the plunger and subsequently to the valve body. A difference in height of the two weld planes causes the initial pre displacement of the spring foil, which pulls the plunger upwards and compresses the soft sealing. The pre displacement is designed to be 100 µm, adding up the difference in height of the plunger and the valve body, and the soft sealing's elevation. The valve body, the plunger, and the spring foil form the impermeable valve chamber. Finally, the actuator foil is laser welded to the valve body.

Blocking of the flow in non-actuated mode is ensured due to the spring foil's restoring force (Fig. 4c). Moreover, a pressure acting on either the spring foil or the plunger induces an additional closing force. Therefore, a fluidic pressure applied on either the valve's inlet or outlet increases sealing of the double normally closed valve. A high voltage on the bending actuator causes the diaphragm, and therefore the plunger, to move downwards. The plunger loses contact to the soft sealing and opens the fluid path (Fig. 4c). Opening takes place as long as the actuator's force is greater than the restoring force of the spring foil.

The initial spring force displacement is crucial for a functioning device, since it determines the balance of sufficient opening in actuated state and low leakage in closed mode. Therefore, the elastic behavior of the spring foil is investigated experimentally

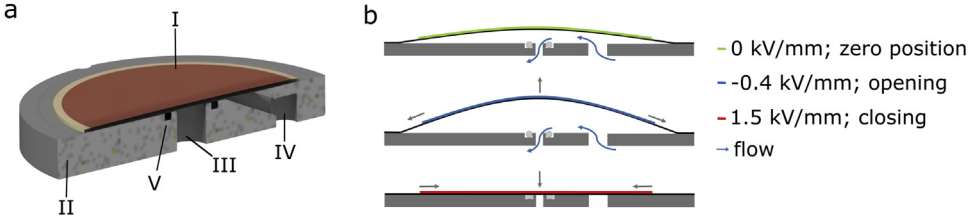

Fig. 3. **a** Model of a normally open valve showing the bending actuator (I), the valve body (II), the outlet (III) and inlet (IV) as well as the FKM sealing (V). **b** working principle. In the non-actuated state, the diaphragm hovers over the sealing, allowing for fluid flow. Using the indirect piezoelectric effect, the valve can be actively opened, further decreasing its fluidic resistance, or actively closed, using a high positive voltage to compress the sealing.

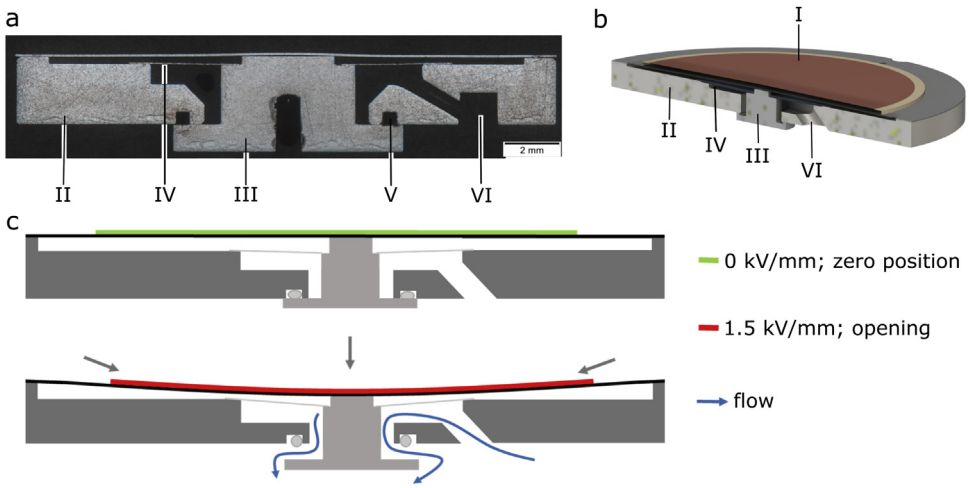

Fig. 4. **a** Section of a normally closed valve showing the valve body (II), the plunger (III), the sealing notch (V) as well as the inlet of the valve (IV).The plunger (III) is welded to a spring foil (IV) and compresses a FKM sealing in the notch (V). **b** model of the valve including the glued on piezo actuator (I). **c** working principle. In non-actuated state, the spring foil pulls the plunger up, closing the valve's outlet. The indirect piezoelectric effect causes the actuator diaphragm to move downwards when a high voltage is applied, which opens the fluid path.

and with finite-element-modelling (FEM) simulation. By variation of the initial spring displacement its effect on the spring force is determined.

3. Materials and methods

For assembly of the novel micropump and valves, we use solely titanium, since it offers high resistance to plastic deformation and is commonly used in medical applications [37]. Rigid parts, such as the pump/valve body, or the plunger of the NC valve, are manufactured using high precision milling. The structured foil components are etched from cold-rolled titanium sheet material of different thicknesses (from 25 μm to 100 μm). Inspecting the topologies of all components ensures flatness of foils, surface smoothness of milled parts, and compliance with geometric requirements. For assembly, foil components are welded to the pump/valve bodies using a fiber laser. The parts are aligned with dowel pins and firmly pressed together to ensure a high-strength bond resulting in hermetic sealing of the devices' chambers. After laser welding, piezo ceramics are mounted using a two-component epoxy glue.

3.1. Stroke measurements

The stroke measurement describes the optical detection of the diaphragm displacement using a quasi-static voltage (amplifier SVR 500−3, piezosystem jena GmbH). Exact movement is determined with a white light profilometer (Fries Research and Technology). The optical sensor has a range of 3 mm and a maximal resolution of 30 nm. The applied voltage passes through the whole range of interest several times to detect the hysteresis as well as initial repolarization of the ceramic. The measurement automation ensures that the time between two recorded voltages is kept constant, minimizing piezoelectric time effects as sources of error. The measurement accuracy of the total actuator stroke is 2 μm, as evaluated from repetitive measurements of several samples.

Furthermore, displacement measurements investigate the NC valve's initial spring tension and elastic behavior. We manufactured four samples specifically for this measurement. The plunger of the valve is not covered with an actuator membrane and can therefore be accessed directly by an applied pressure. A pressure controller (Mensor CPC3000: range -0.5 bar to 2 bar, accuracy: ±0.5 mbar) applies an increasing pressure to the top side of the spring foil, thus forcing a movement of the plunger that is detected optically.

3.2. Fluidic test

We conduct fluidic characterization for each manufactured sample using DI water at room temperature. The sensors used are: Coriflow sensors of different ranges (Bronkhorst MINI CORI-FLOW M14: range 0.5 mL/min to 167 mL/min, accuracy: ± 0.2% and ML120V00: range 0.8 μL/min to 500 μL/min, accuracy: ± 0.2%); a pressure controller (Mensor CPC3000; v.s.) and two piezoresistive pressure sensors (EPCOS Gauge pressure transducers AKR 1.000 C40: range 0.0 bar–1.0 bar, accuracy: ±6 mbar). The latter are placed in the flow path to evaluate the pressure drop over the sample. It is important to notice that the use of coriflow sensors depicts an additional flow resistance in the fluidic path and therefore diminishes the achievable flow rate. Thus, the presented results are the minimal achievable performance.

Micropumps are fluidically characterized by their frequency dependent flow rate at zero backpressure, their pressure dependent flow, and leakage. For evaluations of the frequency dependent flow rate, the pump is actuated with a sinusoidal actuation of -0.4 kV/mm to 1.5 kV/mm. A frequency sweep from 5 Hz to 80 Hz is conducted and the resulting flow recorded after stabilization. All experiments are realized using the same setup, since any changes in the periphery can cause large differences in fluidic performance. Furthermore, pressure dependent flow with 30 Hz sinusoidal actuation is measured. A linear extrapolation of the data enables calculation of the theoretical blocking pressure. We shorten measurement time of the large number of samples by omitting experimental investigations of the blocking pressure. In addition to active flow, we evaluate leakage through the passive check valves with pressure up to 40 kPa.

Fluidic testing of microvalves includes testing of the actuated and non-actuated mode. In our experiments, valves are actuated using a sinusoidal signal with a frequency of f =0.01 Hz and electric fields of -0.4 kV/mm to 2.0 kV/mm. We evaluate the pressure dependent characteristics of an actuated valve for closing and opening lead times. For both actuated and non-actuated valve testing, an applied head pressure is varied using a pressure controller. During open valve testing, the fluid pressure allows a flow through the valve and the flow rate dependent on the electrical field is mea-

sured. For closed valve testing, the pressure dependent leakage through the valve is tested.

3.3. Simulation

For investigation of mechanical tension within the foil components of titanium devices, ANSYS workbench 2019 R1 is used for FEM analysis. Non-linear analysis of large-deformation loads on thin foils is conducted for evaluation of pressure-induced deformations in the elastic regime. This data is compared to mechanical evaluation and crucial for further valve development.

3.4. Data statement

The actuator stroke, fluidic test, and simulation data that support the findings of this study are available in Fordatis – Research Data Repository of Fraunhofer-Gesellschaft with the identifier [https://doi.org/10.24406/fordatis/74] [38].

4. Experimental results and discussion

Medical applications, such as hydraulic implants, require very specific fluidic characteristics. A detailed experimental evaluation is necessary to adapt devices to those requirements and improve the pump and valves further. Table 1 provides an overview of the introduced devices and their fluidic characteristics described hereafter.

4.1. Titanium pump

To assess the titanium pumps' performance, we manufactured a batch of our known steel pumps in parallel to titanium samples and compare the obtained results.

The actuator stroke of a micro diaphragm pump determines the displaced volume per actuation cycle. Optical stroke measurements serve as initial function tests and enable the detection of a touchdown of the diaphragm to the pump chamber bottom, caused by deviations during the piezo mounting process. Fig. 5a displays an example of a titanium pump stroke measurement. The quasi-static actuation is applied from 0.4 kV/mm to 2 kV/mm, covering the operating range as well as an additional positive voltage range for potential touchdown detection. The piezoelectric hysteresis is clearly visible.

The stroke of 24 titanium samples is (79.2 ± 4.3) µm. It is compared to 24 steel pumps' average stroke of (79.8 ± 2.9) µm (Fig. 5b). None of the overall 48 samples exhibit a touchdown. Titanium and steel actuator foils have a thickness of 100 µm. Since titanium is more flexible than steel (Young's modulus of $E_{Ti\text{-}foil}$ =112 GPa compared to $E_{Steel\text{-}foil}$ =195 GPa [39,40]), one expects a higher actuator stroke. Using considerations of Herz et al. [41], we calculated the theoretic difference as approximately 7 µm. Nevertheless, we cannot detect this difference. Other influences such as variations during laser welding, piezo mounting, and deviations in the raw material overlay the influence of the Young's modulus. For instance, incoming goods inspection of the used piezo lot reveals an average thickness of (202 ± 2.8) µm, capacitance of (21.9 ± 0.6) nF and weight of (314 ± 4.4) mg. Comparison of each individual piezo characteristic and device performance reveals no direct dependence. This is due to the sample size of 48 devices, which does not allow to differentiate all influencing parameters.

Fig. 5c shows the measured flow rate of titanium and steel pumps. Both show an initial linear frequency dependence of the flow. Within the linear range, the average flow rate of titanium and steel pumps is alike and reaches up to 11 mL/min. Non-linear behavior starts at approximately 30 Hz, where the inertia of the fluid and passive check valves limits further linear increase and causes a decrease of flow for even faster actuation. The maximal flow is higher for titanium pumps with (14.2 ± 2.5) mL/min compared with (12.2 ± 2.2) mL/min for steel pumps. However, error bars of both groups overlap. The cause for the deviation in maximal flow rate without any difference in the linear regime is not yet solved conclusively. A hypothesis is that the increased elasticity of the spring valves due to the change in material can lead to higher flow rates as inertia effects are less pronounced. It is important to note that the maximal flow strongly depends on the fluidic periphery and pump comparison should always take place in the linear regime.

The flowrate of diaphragm pumps does not only depend on the actuation frequency but also on the applied backpressure. A fixed actuation with increasing backpressure shows a linear decrease in flow (Fig. 5d). Titanium and steel pumps behave very similarly. The extrapolated blocking pressure is approximately 75 kPa. An ideal pump's flow rate is backpressure independent, which can be achieved in further development steps, e.g., with design adaptions [42]. Here, the backpressure dependent flow gives additional information on the micropump's quality. While a pump with poor valves can show reasonable flow without any backpressure, its behavior with pressure is usually deficient. Especially bubble tolerance can suffer, if valves are insufficiently closed. Leakage measurements give further insights on the valve quality. The titanium samples show an average leakage of (0.05 ± 0.04) mL/min with 5 kPa applied to the pumps outlet. This is similar to the steel pumps' leakage of (0.04 ± 0.01) mL/min.

Some characteristics of the individual devices show large variation. While the actuator stroke has a variance of 5%, the flow rate error reaches up to 20% (Fig. 5) and the leakage shows a large scattering with a deviation of up to 80%. The stroke variation can be caused by deviations in raw material characteristics and geometry, such as the piezo characteristics mentioned above. The notably larger scattering of the flow rate is likely due to differences in the valve quality. This hypothesis is substantiated by the extreme scattering of the leakage measurement. A deformed valve that causes large leakage rates allows backflow during the pump stroke and limits the fluidic performance. Such a deformation can be caused by the raw material quality as well as occur during the laser welding process due to heat effects. Not all crucial influences are fully understood yet. We aim to minimize the sample to sample variation in further development steps, considering each individual influence.

The power consumption of the bending actuator is experimentally determined on the pump samples to be 2 mJ/stroke with no dependency on the frequency in the relevant range up to 100 Hz or backpressure conditions. Hence, the pumps' power consumption depends on the frequency and the power per displaced volume depends on the applied pressure. Without applied backpressure, titanium and steel pumps have an energy requirement in the linear regime of 330 J/L. The maximal flow in the non-linear regime requires 420 J/L for titanium pumps and 440 J/L for steel pumps. The resulting power consumption only includes the piezoelectric actuation, while the efficiency of the driving electronics needed to actuate the devices is not taken into account. In general, piezoelectric pumps are considered energy efficient compared to other actuation types [43], however, few authors give exact information. The presented actuator proves to be energy efficient compared to other piezoelectric pumps that require 900 J/L [44] or 1400 J/L [45]. The only pump that requires less energy per displaced volume known to the authors bases on electrostatic actuation and is designed for smaller flow rates and lower backpressure [46].

4.2. Normally open valve

Equivalent to micropump stroke testing, NO valves are tested with a quasi-static actuation from -0.4 kV/mm to 2 kV/mm. Piezo-

Table 1
Overview of design parameters and experimental results of the introduced devices.

	Titanium Pump	Stainless Steel Pump	Normally Open Valve	Normally Closed Valve
Number of tested samples	24	24	24	3
Size in mm^3	Ø20 × 1.5	Ø20 × 1.5	Ø20 × 2.6	Ø20 × 3.6
Driving Voltage in V	−80 to 300	−80 to 300	−80 to 500	−80 to 400
Frequency in Hz	up to 80	up to 80	not applicable	not applicable
Actuator stroke in µm	79.2 ± 4.3	79.8 ± 2.9	57.3 ± 6.3	39.9 ± 4.0
Energy consumption in J/l (linear regime)	330	330	not applicable	not applicable
Energy consumption in J/l (maximal flow rate)	420	440	not applicable	not applicable
Maximal flow rate in ml/min	14.2 ± 2.5	12.2 ± 2.2	not applicable	not applicable
Extrapolated blocking pressure in kPa	75	75	not applicable	not applicable
Leakage at 5 kPa backpressure in µl/min	50 ± 40	40 ± 10	3.4 ± 6.3	2.6 ± 1.9
Open state flow at 20 kPa in ml/min	not applicable	not applicable	27.5 ± 5.3	9.0 ± 9.5
Leakage at 20 kPa in µl/min	not applicable	not applicable	10.9 ± 28.1	0.36 ± 0.15

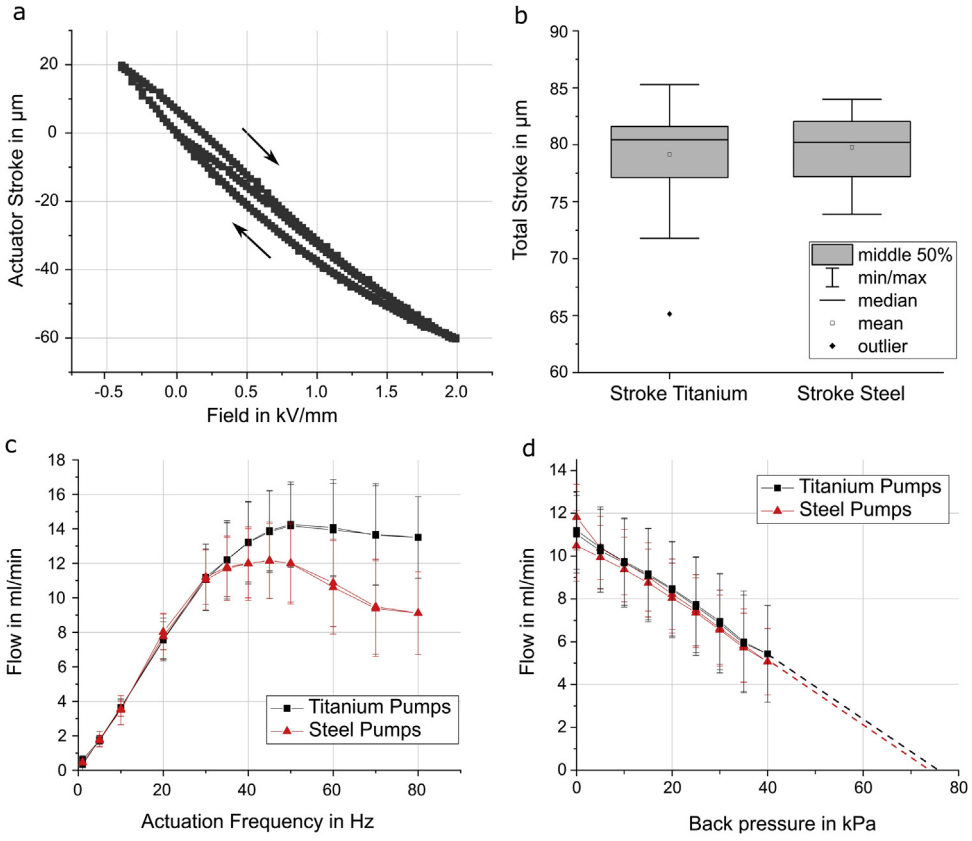

Fig. 5. **a** Typical stroke measurement of a titanium pump. The piezoelectric hysteresis is visible and no touchdown to the pump chamber bottom is detected. **b** box-plot for stroke comparison. The change in material does not cause a change in stroke. **c** average frequency dependent flow rate with no backpressure and sinusoidal actuation of -0.4 to 1.5 kV/mm ($n_{Titanium}$ = 24, n_{Steel} = 24). Both pump types show the same behavior in the linear flow regime. Error bars depict the standard deviation. **d** backpressure capability ($n_{Titanium}$ = 24, n_{Steel} = 24) with sinusoidal actuation of 30 Hz and -0.4 to +1.5 kV/mm. The extrapolated blocking pressure is 75 kPa and does not change with a change in material. Error bars depict the standard deviation.

electric hysteresis as well as the re-polarization initial curve are visible (Fig. 6a). The overall stroke of 24 NO valves is (57.3 ± 6.3) µm. The mechanical blocking of the actuator diaphragm due to the O-ring is clearly visible at approx. 1.3 kV/mm (Fig. 6a). The variance of the stroke is larger for the NO-valves as for the pumps, since the mechanical blocking on the O-ring limits the actuator movement. Due to deviations in O-ring thickness, this actuator blocking occurs at lower or higher actuation voltage.

Fluidic testing of the NO valve includes flow characterization with dynamic actuation (0.1 Hz, sinusoidal waveform) as well as leakage testing with a constant electric field. Fig. 6b shows the opening and closing characteristics of an exemplary NO valve during actuation with 20 kPa head pressure. A strong hysteresis of the passive flow through the valve occurs during actuated mode, which is caused by the piezoelectric hysteresis already observed in stroke measurements, as well as transient flow mechanisms causing fluidic hysteresis. When the electrical field starts to increase from a negative value, the valve is starting to close from its fully opened state. With a high velocity fluid flow being present at full opening, the dynamic pressure within the valve chamber is low during this flow phase. Compared to the opening operation of the valve with a decreasing electrical field, the pre-existing flow field exhibits low velocities and high dynamic pressures. Therefore, the dynamic pressures being present in the valve are different during opening and closing operation, resulting in different flow rates at the same head pressure. The average maximum passive flow of 24 samples is (27.5 ± 5.3) mL/min.

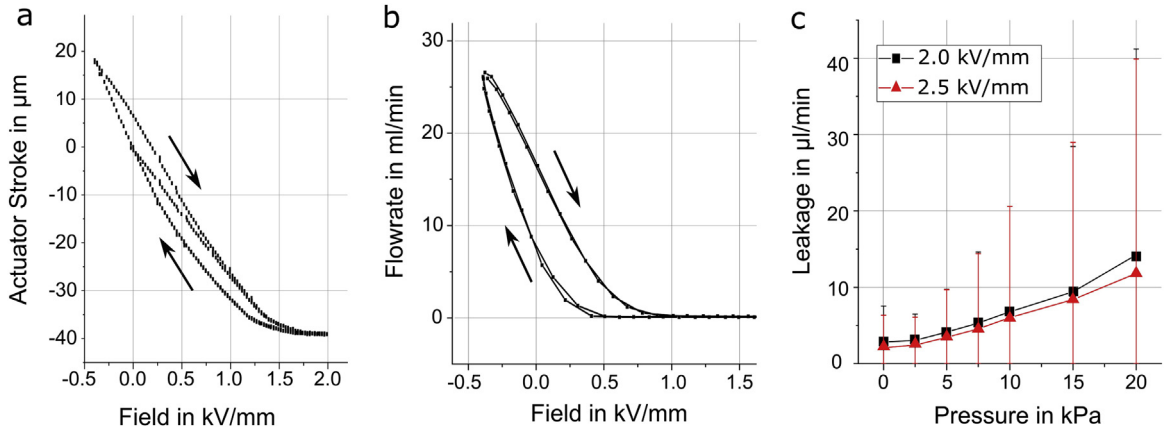

Fig. 6. **a** Typical stroke measurement of a normally open valve. A change in slope is visible at approximately 1.3 kV/mm, when the actuator starts to compress the O-ring creating a large counter force. **b** typical flow characteristic of a normally open valve with 20 kPa head pressure showing complete blockage at approximately 1 kV/mm. Active opening (negative voltage applied) allows a flow of 26 mL/min. **c** average pressure dependent leakage rates of 24 actuated valves at 20 kPa head pressure. Error bars show the standard deviation.

During leakage characterization of NO valves, the actuation field further extends towards positive voltages up to 2.5 kV/mm. This additional field increases the compression of the O-ring by deflecting the diaphragm further. Fig. 6c shows the pressure dependent leakage rates of 24 samples at 2.0 kV/mm and 2.5 kV/mm. The leakages through the tested valves are less than 50 µL/min in the tested pressure range of up to 20 kPa. With an electrical field of 2.0 kV/mm applied, the maximum leakage rate observed is (14.8 ± 27.4) µL/min, while the maximum leakage at 2.5 kV/mm is (10.9 ± 28.1) µL/min. The large sample to sample variation can be caused by geometric differences of the used O-ring. As later characterization shows, the thickness of the O-rings in the used batch varies strongly with (495 ± 33) µm. To further improve leakage rates, the inspection of individual O-rings is planned in future development steps.

4.3. Lifetime investigation normally open valve

An investigation of the piezo lifetime was conducted for micropumps in previous studies [23]. Lifetime evaluations in this study include two devices (NO valve 1 and NO valve 2) to gain first insights whether a shorter lifetime of NO valves is to be expected due to additional mechanical stress (touchdown on the O-ring) compared to micropumps.

A failure due to piezo cracking is detected optically and electrically by measuring the samples' capacitance. A crack decreases the capacitance significantly, since only the electrically contacted part of the piezo is detected.

Prior to life time evaluations, the valves are characterized regarding actuation behavior and leakage. All life time tests are conducted on samples filled with water, and without applied pressure, using sinusoidal actuation, with an electrical field of (-0.2 to +1.9) kV/mm. The valves are actuated at frequencies of [0.1; 1; 2; 10; 20; 50; 100; 275] Hz and 10^4 cycles are driven per frequency step. After each frequency, the capacitance is measured. Finally, the NO valves are driven at 100 Hz until a total amount of one million cycles. Piezo failure was not detected and capacitances remained constant at (14.9 ± 0.2) nF and (15.8 ± 0.3) nF (NO valve No. 1 and No. 2, respectively). Valve performance testing is repeated including stroke measurements, as well as actuation and leakage testing at 20 kPa head pressure. For NO valve No. 2, the change in performance is < 5% (total stroke, leakage rate at p = 20 kPa), whereas the stroke of NO valve No. 1 decreases by 30% and leakage at 20 kPa increases by 100% compared to results right after assembly. The different behavior after lifetime testing is assumed to be under the influence of thickness variation among the O-rings used within the NO valves. For future studies, geometric characterization of the soft sealing in the valves is implemented in order to find correlations to the phenomena observed.

4.4. Normally closed valve

In initial testing, many of the manufactured NC valves showed to be non-functional, since even with high actuation voltages no open state was reached. During failure analysis, we examined the used O-rings regarding their thickness. Their mean thickness deviates significantly from the nominal value of 500 µm and shows large sample-to-sample variation with an average of (585 ± 45.4) µm. Moreover, slightly compensating the increased O-ring thickness, the corresponding sealing notch depth is 50 µm larger as designed. The initial spring displacement is therefore higher than the targeted value of 100 µm, which causes an increase of the spring force and subsequently an imbalance of the forces in the mechanical system. Consequently, the piezoelectric actuator's force is too low to open many of the manufactured valves.

The three functional NC valves are tested for stroke and fluidic performance. Overall stroke of the three NC valves is (39.9 ± 4.0) µm with a quasi-static actuation of 0.4 kV/mm to 2 kV/mm. Fig. 7a shows a typical stroke measurement of one exemplary valve. The slope is steep for negative voltages, where the actuator diaphragm is not in contact with the plunger. This part of the curve characterizes the mechanical behavior of the bending actuator. A change in slope occurs at the touchdown of the diaphragm to the plunger (Fig. 7a). The counter force of the spring foil attached to the plunger reduces possible movement.

Fluidic testing of the NC valve includes flow characterization with actuation as well as leakage testing during non-actuated mode at 20 kP head pressure. Leakage through all three tested valves is less than 1 µL/min with an average of (0.36 ± 0.15) µL/min. This is in good accordance with the designed high O-ring compression enabling a tight seal. Fig. 7b depicts the opening and closing characteristics of a NC valve in actuated mode. Same as for NO valves, a fluidic hysteresis occurs due to piezo hysteresis and dynamic pressure differences. The average maximum flow of three samples at 20 kPa head pressure is (9.0 ± 9.5) mL/min.

4.5. Spring foil investigation normally closed valve

The elastic deformation of the NC valve's spring foil is crucial for its functionality. Therefore, we conduct an experimental and

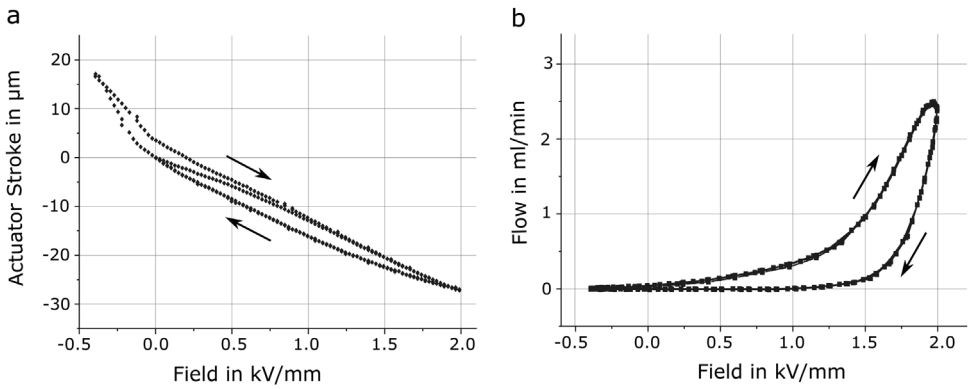

Fig. 7. **a** Typical stroke measurement of a normally closed valve. A change in slope is visible at approximately -0.2 kV/mm, when the actuator diaphragm loses touch to the plunger. **b** typical flow characteristic of a normally closed valve at 20 kPa pressure difference showing a blockage of the fluid flow up to 0.25 kV/mm and a maximal flow in open state of 2.5 mL/min with 20 kPa pressure applied.

numerical investigation. A comparison of the data enables targeted design changes to achieve desired opening and leakage behavior.

A half model of the spring foil (thickness of 50 µm) is investigated and a fine, structured hexagonal mesh is implemented (Fig. 8a). A pressure load is applied to the inner area, which is the interface of the spring foil and the plunger (Fig. 8b). This inner area (C, yellow), which is welded to the plunger, can solely move in z direction, while movement in x or y direction is suppressed in order to comply with the physics of the weld. The area of the outer weld line connecting the foil to the valve body is defined as a fixed support (A, blue). It is restrained in all six degrees of freedom. Boundary condition B (red) is the applied pressure load that leads to a displacement by elastic deformation of the structure. Fig. 8c shows the deformation in true scale, with z-displacement presented in false color.

We evaluate the spring foil deformation under pressure load with regard to an initial spring displacement (Fig. 8d). The dotted curves show the pressure dependent behavior starting at a given displacement by forcing an inner ring position in order to imitate the initial displacement during manufacturing. The solid line depicts experimental results. It is evident from the FEM data that the displacement depends strongly on the initial spring displacement after laser welding. Higher initial displacement leads to stiffer behavior of the foil.

Experimental data is in good agreement with the FEM data assuming a 120 µm initial spring displacement. The increased O-ring elevation of 35 µm can cause such a shift from the designed 100 µm initial displacement to 120 µm when assuming O-ring compression, which was not individually evaluated for each device in this study. The total stroke of the spring foil at 100 kPa pressure load is below 20 µm for a high initial spring displacement (120 µm) in numerical evaluations as well as for experimental results. Such a low displacement of the spring foil and the plunger leads to a low decompression of the O-ring, not opening the valve. Further improvement of the design and adaptation of O-rings is necessary. A displacement of 40 µm or more, which allows full opening, in the blocking pressure range of the piezoelectric actuator of roughly 80 kPa is possible for an initial spring displacement of 50 µm. Therefore, design parameters need adaptation towards lower initial spring tension.

5. Conclusion

This work summarizes the development and evaluation of a titanium based microfluidic platform for medical applications. The combination of the piezoelectric micropump, a NC as well as a NO microvalve offers many possibilities to develop small and energy efficient implants with broad functionality and automated control instead of manual operation.

The titanium micropumps show promising results. With (79.2 ± 4.3) µm, their stroke height is similar to comparable steel pumps showing (79.8 ± 2.9) µm of stroke. The flow characteristics of both pump types are alike, which matches their similar stroke. Within the linear regime, the novel titanium pumps reach an average flow of (11 ± 2) mL/min. The average maximal flow of the 24 samples is (14.2 ± 2.5) mL/min and thereby 2 mL/min higher than the one of the steel samples. The backpressure capability is also very promising, showing an extrapolated blocking pressure of 75 kPa.

In this work, we also describe the development and evaluation of new titanium NO valves. Even though they use the same actuator, the valves show a smaller stroke of (57.3 ± 6.3) µm as compared to the titanium pumps, since a touchdown to the O-ring blocks further membrane movement. Leakage rates of all 24 samples are in an acceptable range below 50 µL/min. The sample-to-sample variation of leakage is rather high with an average of (10.9 ± 28.1) µL/min. Further improvement to minimize variations is necessary and possible. Nonetheless, already good closing behavior is achieved and many samples exhibit low leakage, proofing the feasibility of this device. Free flow is evaluated for 20 kPa head pressure, which is a realistic pressure the pump easily provides. The high flow of (27.5 ± 5.3) mL/min displays a low flow resistance, which is important for efficient system architecture.

In the NO valve, premature failure can occur due to the touchdown of the actuator membrane on the O-ring, which causes a different strain distribution within the piezo ceramic compared to the pumps where the membrane can move freely. Preliminary lifetime tests on two samples showed no piezo failure within one million cycles. However, fluidic performance changed unreproducibly, making further design considerations and lifetime testing necessary.

Manufacturing of functional NC valves posed problems, since extremely low tolerances of all parts are necessary. The large deviation in O-ring thickness observed leads to a too high initial spring tension acting on the plunger and a resulting high spring force countering piezo-actuator movement. Therefore, only three out of thirty samples showed valve functionality, while all others stayed constantly closed. Comparison of measured O-ring thicknesses and FEM simulation are in good agreement and indicate that slight design changes can increase the yield of working valves tremendously. The three functioning samples show very promising results. Leakage in closed (non-actuated) mode is extremely low with (0.36 ± 0.15) µL/min.

The introduced titanium platform offers great possibilities for microfluidic applications, especially in the medical field. The pre-

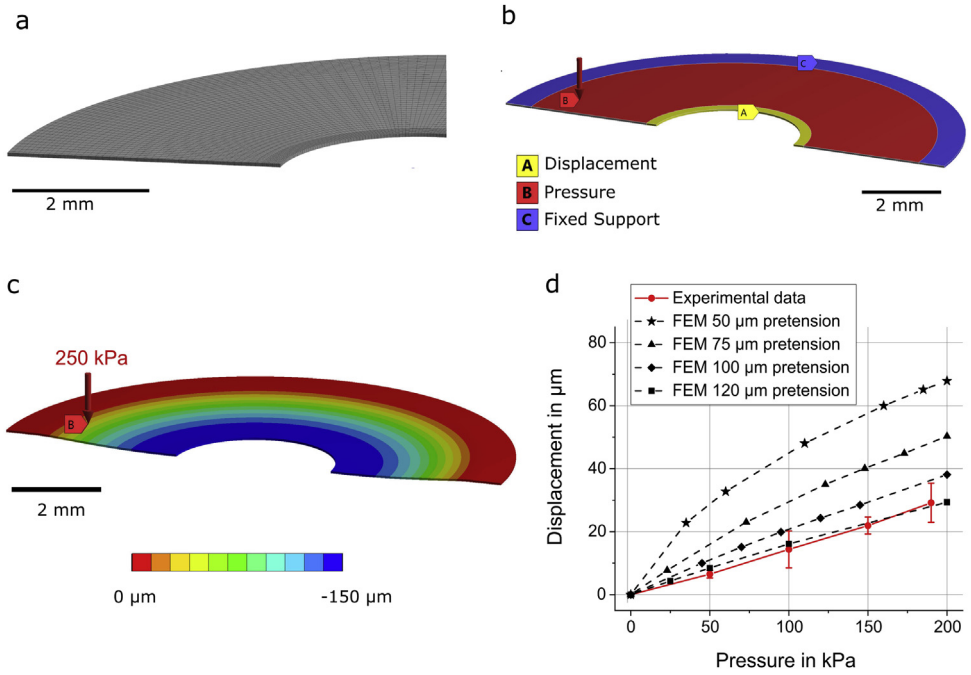

Fig. 8. **a** Half model of the spring foil with structured mesh. **b** boundary conditions. The outer ring (C) is set as fixed support and the displacement of the inner ring (A) is evaluated with a given pressure applied to area B. **c** deformed model in true scale for a pressure of 250 kPa. **d** experimental and FEM results of the spring foil's displacement under pressure load. With 50 µm initial displacement, the numerical solution differs strongly from the experimental results, while a calculation using 120 µm pre-displacement shows fitting results.

sented pump combines high flow rates with high backpressure abilities. We designed and tested microvalves with low leakage rates and high free flow, making them suitable for reliable flow restrictors with low fluidic resistance in open state. Additionally, we showed possibilities for further improvement. All devices consist only of titanium, FKM sealing, and a glued on piezo ceramic, achieving MRI-compatibility. In addition, compatibility with a large variety of fluids is given since all wetted surfaces are titanium or FKM. Especially for medical applications, energy efficiency can be a crucial property. Piezoelectric actuation offers an energy efficient as well as space saving actuation method for both pumps and valves. Furthermore, the similar form factor of the devices enable easy and space efficient combination. The choice between NC and NO valves makes it possible to design well-adapted systems with the lowest possible energy consumption. The introduced devices are the base of a microfluidic titanium-based technology platform. The aim of future research is to further develop existing devices and extend the functionality of the platform further.

CRediT authorship contribution statement

Agnes Beate Bußmann: Conceptualization, Data curation, Formal analysis, Investigation, Methodology, Project administration, Resources, Validation, Visualization, Writing - original draft, Writing - review & editing. **Claudia Patricia Durasiewicz:** Data curation, Formal analysis, Investigation, Methodology, Project administration, Resources, Validation, Writing - original draft, Writing - review & editing. **Sebastian Heinrich Alexander Kibler:** Funding acquisition, Supervision, Methodology, Validation, Writing - review & editing. **Christian Klaus Wald:** Funding acquisition, Methodology, Supervision, Validation, Writing - review & editing.

Declaration of Competing Interest

The authors report no declarations of interest.

Acknowledgements

This work was partly funded by the "Bayrische Forschungsstiftung" within the project "Aktive, theranostische Blasenschließmuskeltechnologie" (active, theranostatic bladder sphincter technology) as well as the Federal Ministry of Education and Research [project reference numbers 16FMD01K, 16FMD02, and 16FMD03].

All authors have read and agreed to the published version of the manuscript.

References

[1] C.W. Jenke, S. Kibler, Y. Gao, A. Hollot, T. Neuhann, B. Kirchhof, B. Montag, M. Geiger, J. Neitzel, C. Kutter, M. Richter, Optimiation of a piezoelectric micropump actuator for medical application in glaucoma and phthisis therapy, Actuator 2014, 14th International Conference on New Actuators & 8th International Exhibition on Smart Actuators and Drive Systems. Conference Proceeding (2014).

[2] L. Marziale, G. Lucarini, T. Mazzocchi, E. Gruppioni, S. Castellano, A. Davalli, R. Sacchetti, D. Pistolesi, L. Ricotti, A. Menciassi, Artificial sphincters to manage urinary incontinence: a review, Artif. Organs 42 (2018) E215–E233, http://dx.doi.org/10.1111/aor.13164.

[3] H. Anhalt, N.J. Bohannon, Insulin Patch Pumps: Their Development and Future in Closed-Loop Systems, DIABETES TECHNOLOGY & THERAPEUTICS, 2010.

[4] A. Kargov, T. Werner, C. Pylatiuk, S. Schulz, Development of a miniaturised hydraulic actuation system for artificial hands, Sens. Actuators A Phys. 141 (2008) 548–557.

[5] P. Solanki, Aortic counterpulsation: C-pulse and other devices for cardiac support, J. Cardiovasc. Transl. Res. 7 (2014) 292–300, http://dx.doi.org/10.1007/s12265-014-9548-6.

[6] S. Siracusano, L. Fondacaro, E. Melega, Artificial urinary (AUS) and anal (AAS) sphincter, in: S. Siracusano, G. Dodi, M. Pennisi, C. Gozzi, A.L. Pastore, M.A. Cerruto (Eds.), Complications of Surgery for Male Urinary and Fecal Incontinence, Springer International Publishing, Cham, 2020, pp. 43–53.

[7] H.-J. Schrag, F.F. Padilla, A. Doll, F. Goldschmidtböing, P. Woias, U.T. Hopt, German Artificial Sphincter System-GASS: development of a novel and highly integrated sphincter prosthesis for therapy of major fecale incontinence based on piezotechnology, Biomed. Eng./Biomedizinische Technik 49 (2004) 273–277, http://dx.doi.org/10.1515/BMT.2004.051.

[8] M.V. Sefton, H.M. Lusher, S.R. Firth, M.U. Waher, Controlled release micropump for insulin administration, Ann. Biomed. Eng. 7 (1979) 329–343, http://dx.doi.org/10.1007/BF02364120.

[9] D.J. Laser, J.G. Santiago, A review of micropumps, J. Micromech. Microeng. (2004) R35–R64.
[10] S. Mohith, P.N. Karanth, S.M. Kulkarni, Recent trends in mechanical micropumps and their applications: a review, Mechatronics 60 (2019) 34–55, http://dx.doi.org/10.1016/j.mechatronics.2019.04.009.
[11] Y.-N. Wang, L.-M. Fu, Micropumps and biomedical applications – a review, Microelectron. Eng. 195 (2018) 121–138.
[12] A. Chandrasekaran, M. Packirisamy, Experimental investigation of cavitation behavior in valveless micropumps, J. Micromech. Microeng. 22 (2012) 125019, http://dx.doi.org/10.1088/0960-1317/22/12/125019.
[13] M. Richter, R. Linnemann, P. Woias, Robust design of gas and liquid micropumps, Sens. Actuators A Phys. 68 (1998) 480–486.
[14] M. Herz, M. Richter, M. Wackerle, Method for manufacturing a bending transducer, a micro pump and a micro valve, micro pump and micro valve, Google Patents, 2016.
[15] K. Oh, C. Ahn, A review of microvalves, J. Micromech. Microeng. 16 (2006) 13–39.
[16] J.-Y. Qian, C.-W. Hou, X.-J. Li, Z.-J. Jin, Actuation mechanism of microvalves: a review, Micromachines 11 (2020) 172.
[17] S. Zaehringer, M. Menacher, P. Kirchner, N. Schwesinger (Eds.), Design of a Normally Closed Piezoelectric Micro Valve (2010).
[18] P.V. Ramanamurthy, R. Ahrens, S. Karmalkar, Piezoelectric Microvalve, 2007, pp. 0019–5596.
[19] Eui-Hyeok E.H. Yang, Choonsup Lee, Juergen Mueller (Eds.), Normally-Closed, Leak-Tight Piezoelectric Microvalve Under Ultra-High Upstream Pressure for Integrated Micropropulsion, IEEE, 2003.
[20] T. Rogge, Z. Rummler, W.K. Schomburg, Polymer micro valve with a hydraulic piezo-drive fabricated by the AMANDA process, Sens. Actuators A Phys. 110 (2004) 206–212.
[21] S. Chen, S. Lu, Y. Liu, J. Wang, X. Tian, G. Liu, Z. Yang, A normally-closed piezoelectric micro-valve with flexible stopper, AIP Adv. 6 (2016) 45112.
[22] C. Wald, Martin Richter, Low-Cost Stainless Steel Micro Pumps for miniaturized early fire detection systems, MikroSystemTechnik Kongress 2015; 26. - 28. October 2015 in Karlsruhe; proceedings, VDE-Verl., Berlin, 2015.
[23] A. Bussmann, L. Gruenerbel, Increasing piezo micro diaphragm pump performance by optimizing piezo actuation, smart systems integration, Conference Proceedings (2019) 1–4.
[24] R. Buchli, P. Boesiger, D. Meier, Heating effects of metallic implants by MRI examinations, Magn. Reson. Med. 7 (1988) 255–261.
[25] A. Holton, E. Walsh, A. Anayiotos, G. Pohost, R. Venugopalan, Comparative mri compatibility of 316l stainless steel alloy and nickel–titanium alloy stents: original article technical, J. Cardiovasc. Magn. Reson. 4 (2002) 423–430.
[26] A. Klocke, J. Kemper, D. Schulze, G. Adam, B. Kahl-Nieke, Magnetic field interactions of orthodontic wires during magnetic resonance imaging (MRI) at 1.5 Tesla, J. Orofacial Orthoped./Fortschritte der Kieferorthopädie 66 (2005) 279–287.
[27] D.M. Brunette, P. Tengvall, M. Textor, P. Thomsen, Titanium in Medicine: Material Science, Surface Science, Engineering, Biological Responses and Medical Applications, Springer Science & Business Media, 2012.
[28] A.T. Sidambe, Biocompatibility of advanced manufactured titanium implants—a review, Materials 7 (2014) 8168–8188, http://dx.doi.org/10.3390/ma7128168.
[29] A.M. Khorasani, M. Goldberg, E.H. Doeven, G. Littlefair, Titanium in biomedical applications—properties and fabrication: a review, J. Biomater. Tissue Eng. 5 (2015) 593–619, http://dx.doi.org/10.1166/jbt.2015.1361.
[30] G. Jiang, D.D. Zhou, Technology advances and challenges in hermetic packaging for implantable medical devices, in: D. Zhou, E. Greenbaum (Eds.), Implantable Neural Prostheses 2, Springer, New York, New York, NY, 2010, pp. 27–61.
[31] E. Blasco-Tamarit, A. Igual-Muñoz, J.G. Antón, D.M. García-García, Galvanic corrosion of titanium coupled to welded titanium in LiBr solutions at different temperatures, Corros. Sci. 51 (2009) 1095–1102, http://dx.doi.org/10.1016/j.corsci.2009.02.023.
[32] K. Nakahara, M. Yamamoto, Y. Okayama, K. Yoshimura, K. Fukagata, N. Miki, A peristaltic micropump using traveling waves on a polymer membrane, J. Micromech. Microeng. 23 (2013) 85024, http://dx.doi.org/10.1088/0960-1317/23/8/085024.
[33] R. Rapp, Schomburg, W.K. Schomburg, J. Schulz, W. Stark, LIGA micropump for gases and liquids, Sens. Actuators A Phys. 40 (1994) 57–61, http://dx.doi.org/10.1016/0924-4247(94)85030-5.
[34] G. Liu, C. Shen, Z. Yang, X. Cai, H. Zhang, A disposable piezoelectric micropump with high performance for closed-loop insulin therapy system, Sens. Actuators A Phys. 163 (2010) 291–296, http://dx.doi.org/10.1016/j.sna.2010.06.030.
[35] T. Guo, T. Meng, W. Li, J. Qin, Z. Tong, Q. Zhang, X. Li, UV-driven microvalve based on a micro–nano TiO2/SiO2 composite surface for microscale flow control, Nanotechnology 25 (2014) 125301.
[36] M. Herz, M. Richter, M. Wackerle, Method for manufacturing a bending transducer, a micro pump and a micro valve, micro pump and micro valve, Google Patents, 2016.
[37] C. Veiga, J.P. Davim, A.J.R. Loureiro, Properties and applications of titanium alloys: a brief review, Rev. Adv. Mater. Sci. (2012) 133–148.
[38] C. Durasiewicz, A. Bußmann, S. Kibler, C. Wald, Experimental Characterisation and Simulation of Piezoelectric Titanium Micropumps and Titanium Microvalves, Fordatis - Research Data Repository of Fraunhofer-Gesellschaft, 2019, pp. 2019, http://dx.doi.org/10.24406/fordatis/74.
[39] C. Leyens, M. Peters, J. Kumpfert, Titanium and Titanium Alloys: Fundamentals and Applications, Wiley & Sons, 2003.
[40] Z. Chen, U. Gandhi, J. Lee, R. Wagoner, Variation and consistency of Young's modulus in steel, J. Mater. Process. Technol. 227 (2016) 227–243, http://dx.doi.org/10.1016/j.jmatprotec.2015.08.024, January 2016, 227.
[41] M. Herz, D. Horsch, G. Wachutka, T.C. Lueth, M. Richter, Design of ideal circular bending actuators for high performance micropumps, Sens. Actuators A Phys. 163 (2010) 231–239.
[42] E. Chappel, S. Mefti, G.-L. Lettieri, S. Proennecke, C. Conan, High Precision Innovative Micropump for Artificial Pancreas, in: Microfluidics, BioMEMS, and Medical Microsystems XII, SPIE, San Francisco, California, United States, 2014, pp. 89761C.
[43] S. Ogden, L. Klintberg, G. Thornell, K. Hjort, R. Bodén, Review on miniaturized paraffin phase change actuators, valves, and pumps, Microfluid Nanofluid 17 (2014) 53–71, http://dx.doi.org/10.1007/s10404-013-1289-3.
[44] P.-H. Cazorla, O. Fuchs, M. Cochet, S. Maubert, G. Le Rhun, Y. Fouillet, E. Defay, A low voltage silicon micro-pump based on piezoelectric thin films, Sens. Actuators A Phys. 250 (2016) 35–39, http://dx.doi.org/10.1016/j.sna.2016.09.012.
[45] A.F. Doll, M. Wischke, A. Geipel, F. Goldschmidtboeing, O. Ruthmann, U.T. Hopt, H.-J. Schrag, P. Woias, A novel artificial sphincter prosthesis driven by a four-membrane silicon micropump, Sens. Actuators A Phys. 139 (2007) 203–209, http://dx.doi.org/10.1016/j.sna.2007.03.025.
[46] R. Zengerle, J. Ulrich, S. Kluge, M. Richter, A. Richter, A bidirectional silicon micropump, Sens. Actuators A Phys. 50 (1995) 81–86, http://dx.doi.org/10.1016/0924-4247(96)80088-4.

Biographies

Agnes Bußmann, M. Sc. received her Master of Science in Mechanical Engineering from TU Munich in 2017. During her research stay in France she investigated failure mechanisms of vascular prosthesis. She currently works as a development engineer at the Fraunhofer Research Institution for Microsystems and Solid State Technologies EMFT and pursues her doctorate in cooperation with the Institute of Engineering in Life Sciences of the Karlsruhe Institute of Technology. Her research focusses on piezoelectric micro diaphragm pumps and their biomedical application.

Claudia Durasiewicz, M. Sc. graduated at the Technical University of Berlin with a Master degree in Engineering Science specializing in fluid mechanics. During her studies she worked in the field of medical device development, e.g. studies of flow phenomena in an innovative VAD system. As a visiting scholar at the University of Arizona she investigated plasma-actuation of the flow around an airfoil on a nanosecond scale. She joined the department for Micro Dosing Systems at the Fraunhofer EMFT in October 2017. In her doctorate work she focuses on microscale process technologies for micropump and microvalve development.

Dr.-Ing. Sebastian Kibler studied Electrical Engineering and Information Technologies at the TU Munich and received his diploma in 2008. He joined the Fraunhofer EMFT Team of Micro Dosing Systems in 2008 to work in the field of system development of micro dosing systems. Within his work on feedback-controlled micro dosing for nanoliter oil lubrication, he finished his doctoral degree at the Bundeswehr University Munich in 2017. As head of the Systems and Implants group he focuses on the management of system and component development of micro fluidic actuators and dosing units for implantable medical applications.

Christian Wald, Dipl.-Wirtsch.-Ing. studied Industrial Engineering at the Karlsruher Institute for Technology KIT and got his diploma in 2010. He joined the Fraunhofer EMFT Team of Micro Dosing Systems in 2011 and worked in the field of medical devices (negative pressure wound therapy, infusion) and industrial applications (water analysis, vaporizer, gas- and smoke detection and fuel cells). Focus of his work are the metal micropump development and business development. In 2015 he became Deputy Quality Manager of the Fraunhofer EMFT and in 2018 Deputy Department Manager of the Micro Dosing Systems team.